



D2.4 | Heat engine efficiency

Author(s): C. I. L. de Araujo, E. Strambini

Delivery date: 28.02.2023

Version: 1.0



| | |
|---------------------|--|
| Project Acronym: | SUPER TED |
| Project Full Title: | Thermoelectric detector based on superconductor-ferromagnet heterostructures |
| Call: | H2020-FETOPEN-2016-2017 |
| Topic: | FETOPEN-01-2016-2017 |
| Type of Action: | RIA |
| Grant Number: | 800923 |
| Project URL: | https://superted-project.eu/ |

| | |
|----------------------------|--|
| Editor: | C. I. L. de Araujo, CNR Pisa; E. Strambini, CNR Pisa |
| Deliverable nature: | Report (R) |
| Dissemination level: | Public (PU) |
| Contractual Delivery Date: | 28.02.2023 |
| Actual Delivery Date: | 28.02.2023 |
| Number of pages: | 7 |
| Keywords: | Superconducting thermoelectric detector, Thermoelectric effect, Thermoelectric power generation, Tunneling spectroscopy |
| Author(s): | C. I. L. de Araujo, CNR Pisa M. Spies, CNR Pisa E. Strambini, CNR Pisa |
| Contributor(s): | T. T. Heikkilä, JYU P. Virtanen, JYU C. G. Orellana, CSIC M. Ilyn, CSIC C. Rogero, CSIC Sanna Rauhamäki, JYU F. Giazotto, CNR Pisa |
| External contributor(s): | |

Abstract

The present report on Deliverable D2.4 ‘Heat engine efficiency’ of Work Package 2 gives an overview of the experimental results obtained in the last period of the project: the quantification of thermal power converted into electrical power via the thermoelectric effect. The ferromagnetic insulator (FI) - superconductor (S) tunnel junctions have been designed to maximize the thermoelectric component with respect to the rectifying one.

1 Introduction

The central building block of the superconducting thermoelectric detector of the EU Horizon 2020-funded SuperTED project is the quantification of the thermoelectric component of the spin-split ferromagnetic tunnel junctions [1] used in proposed detectors. A giant thermoelectric response has been predicted [2] for such ultra-sensitive radiation detectors [3]. These detectors are “self-powered” thanks to the incoming radiation, i.e., the detector signal arises from absorbed radiation, and no bias is needed. They are hence different from the presently pursued concepts of transition edge sensors [4] and kinetic inductance detectors [5], that require a bias for their read-out. The lack of bias lines simplifies the construction of the detector, allows for bigger detector arrays and allows getting rid of the bias-induced heating that has an adverse effect on the detector resolution.



This project has received funding from the European Union’s Horizon 2020 research and innovation programme under grant agreement No 800923.

In the Deliverable 2.4 we quantify the effective power that can be extracted from such a thermoelectric effect. Knowing the efficiency of the heat-to-power conversion (heat engine) is essential for the design of the "self-powered" read-out circuit at the base of SuperTED detector. In the previous Deliverable 2.3 of the project, we understood that in FI/S-based tunnel junctions both thermoelectricity and rectification are present as the two concomitant phenomena are originating from the same electron-hole symmetry breaking. We then used said knowledge to optimize the design of the sample geometry in order to enhance the thermoelectricity with respect to rectification and to avoid negative competing effects.

In the first part of this Deliverable report, we present the tunneling spectroscopy of the new generation of EuS/Al/AlO_x/Co samples from CSIC. The resistance of the tunnel barrier was increased to minimize the leakage of the heating current into the Al leads and the resulting rectification signals. In the second part, we describe the set-up that was used to measure the thermoelectric voltage and power generated on a load resistor in order to quantify the heat-engine efficiency. Such heat to power conversion realizes the first heat-engine based on a superconducting spin-selective tunnel barrier.

The main experimental findings will be discussed without presenting the data to avoid copyright conflict with the publication process of the work. Additional information, including data, will be confidentially provided to the reviewers upon request. Furthermore, in agreement with the Green open-access policy of the SUPERTED project, a draft of the publication containing all the data and sample information is expected to be available in the arXiv.org repository at the end of March 2023.

1.1 Device characterization

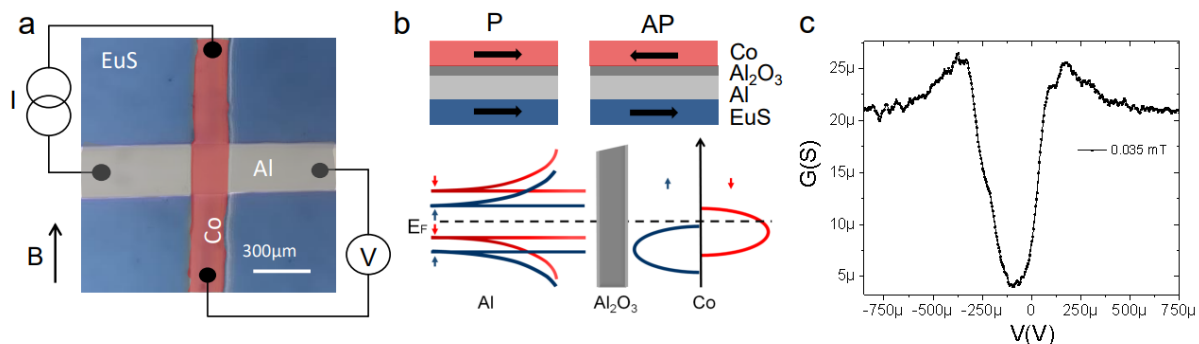


Figure 1: a) Optical microscope image of the sample measured. It consist of crossbars made of: a EuS layer (blue) on top of a Si/SiO substrate, an Al strip (grey) defined by a shadow mask and oxidized in an oxygen argon environment for 5h, followed by a Co strip (red), likewise defined by a shadow mask. The entire sample was covered by a 3nm CaF capping layer for protection. The circuit shows the 4 point probe measurement utilized and the magnetic field direction which is parallel to the Co strip. b) Scheme of the sample side view (top) and simplified representation of device density of states (bottom), with spin split Al superconducting gap (left) and spin polarized Co 3d bands (right). c) Differential conductance as a function of voltage at 35 mT and 100 mK bath temperature.

In Fig. 1a an optical false color microscope image of a typical device is shown together with the four-wire measurement scheme used for the tunneling spectroscopy characterization. First, a film of 12.5 nm EuS is grown by molecular beam epitaxy on top of *Si/SiO_x* substrates. In the second step, a shadow mask is utilized to define a 20 nm Al strip. The tunnel barrier was developed on top of the Al strip by oxidation of the Al layer for 5 hours. The subsequent cross bar geometry was achieved by use of another shadow mask for definition of 14 nm of Co. The



protection against environmental oxidation was performed on top of the whole system by a 3nm CaF insulator layer.

Samples were wire bonded with Al wires and mounted in a dilution fridge, where the electrical measurements were performed through low pass and high pass filters. All the signals were amplified by utilization of low noise voltage and current amplifiers. For the amplification of the heating currents and the measurements of the critical currents, the filters were bypassed, in order to decrease the power loss that would excessively heat the cryostat. The tunneling conductance of the device $G(V)$ was obtained from the numerical derivative of the measured current-voltage characteristics ($I(V)$).

$G(V)$ is strongly dependent on the spin-splitting of the superconductor density of states (DOS) and the spin-filtering induced by the Co counter-electrode as described in the simplified energy model for the FI/S/I/F tunnel junction presented in the cartoon of Fig. 1b. The tunneling conductance G measured at 35 mT and 100 mK is presented in Fig. 1c. The characteristic asymmetry in $G(V)$ is compatible with a parallel (P) alignment of the magnetization directions of the EuS and Co layers and is visible for most of the fields explored. Only the $B \simeq 10$ mT tunneling conductance is characterized by an anti-parallel (AP) alignment of the two layers (not shown). By numerical fitting of the presented experimental data [6], we were able to extract the polarization of the Co layer $P = 0.3$ and the exchange interaction $h_0 = 0.025\Delta$, with $\Delta = 350 \mu\text{V}$. Notably, the tunneling resistance is much higher than previous devices based on EuS tunnel barriers [7]. That way, the transversal rectification reported in the Deliverable 2.3 is largely prevented. This is also confirmed by the theoretical model reported in Sec.3 of Deliverable 2.3 and in the supplementary material of ref [7] which estimates a critical length of $L_C \simeq 10$ nm, which is much longer than the lateral size of the junction $\sim 150\mu\text{m}$.

2 Results and Discussions

2.1 Thermovoltage

By changing the circuit to an open voltage measurement configuration, we aim at measuring the predicted thermoelectric voltage drop across the junction as a function of temperature difference between the Co and Al electrodes. Such temperature difference is achieved by heating currents I_H applied on the Co strip while the Al is kept at bath temperature due to its thermal coupling with the substrate (see scheme presented in Fig. 1a).

To extract the thermovoltage signal (V_{th}) from the voltage measurement, both positive and negative heating currents are applied after one another and V_{th} is evaluated by simple voltage symmetrization $V_{th} = \frac{V(+I_H) + V(-I_H)}{2}$. This procedure allows removing the trivial Ohmic, anti-symmetric component of $V(I_H)$ originating from the shared paths between the current source and the voltage probe.

After the symmetrization, a clear monotonic increase of $V_{th}(I_H)$ is visible with a slope of $dV_{th}/dI_H \simeq 0.5\Omega$ up to a saturation of $\simeq 15\mu\text{V}$ observed above $I_H = 30\mu\text{A}$. For such a high dissipated power, the temperature in the Al strip starts to visibly increase as confirmed by additional measurements of the Al critical currents by Co input heating. On the other hand, the Co temperature is estimated as a function of I_H by measuring the tunneling spectroscopy of the junction at different values of I_H . The broadening of the tunneling spectroscopy can be directly correlated to the temperature of the Co electrode, both by simple fitting with a theoretical model or from the direct comparison to the tunneling spectroscopy measured at different bath temperatures. From such analysis we extrapolated the temperature gradient across the junction vs. the heating current ($\delta T(I_H)$). For a bath temperature of 200 mK an



almost linear dependence of $\delta T(I_H)$ was observed with a slope of $\sim 15 \frac{mK}{\mu A}$ up to $50 \mu A$, which is in good agreement with the thermal model of the device. From such temperature calibration, it is possible to extract the $V_{th}(\delta T)$ curve and estimate a Seebeck coefficient as large as $30 \frac{\mu V}{K}$. This is 0.35 times the "fundamental" scale k_B/e .

Notably, a negative thermovoltage was observed in the AP state obtained at $B = -10mT$. That result represents the first observation of superconducting n-type and p-type Seebeck effect and could be useful for further technological application in arrays of junctions to improve sensing. The thermovoltage measured at different temperatures showed a robustness in temperature with a sizable thermovoltage ($\simeq 5 \mu V$) observed still above 800 mK. The field dependence shows consistently thermovoltage signals up to 120mT with the damping of the superconductivity observed in the tunneling conductance shown Figure 1 c.

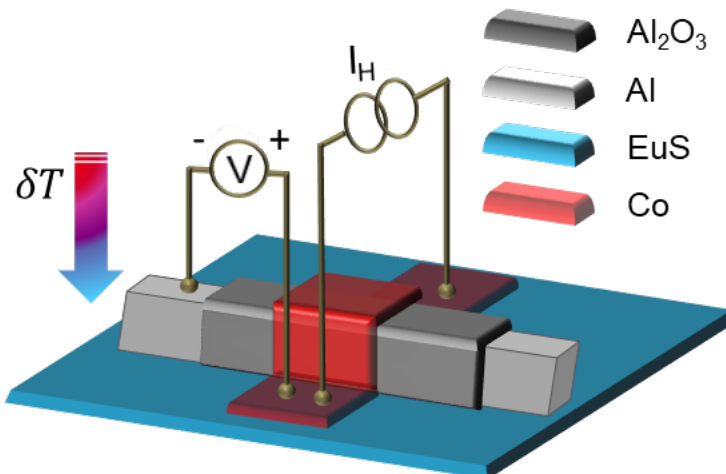


Figure 2: a) Schematics for the thermovoltage measurement. The heating current I_H is injected in the Co strip to generate the thermal bias across the tunnel junction. The voltage drop across the junction is measured. The thermoelectric voltage is separated from the Ohmic component induced by the common path shared with I_H by symmetrization $V_{th} = (V(I_H) + V(-I_H))/2$.

2.2 Heat Engine

In this section we discuss the main result of this Deliverable, which is the heat engine effect in the superconducting ferromagnetic tunnel junctions investigated. To extract the power from the thermoelectric effect, the thermovoltage is applied to a variable load resistance (R_L). By measuring the load voltage (V_L) the resulting dissipated power is extracted $P_L = \frac{V_L^2}{R_L}$ according to the circuital scheme used for the measurement shown in Fig 3. To prevent unwanted leak currents from I_H in to the load resistor two balance resistors ($R_B = 10k\Omega$) have been inserted into the circuit. The impedance of the balance resistor was selected to be negligible with respect to the load resistor ($R_B \ll R_L$) in order to be able to neglect the power loss in the balance circuit with respect to P_L . By fixing the heating current to $40 \mu A$, which corresponds to a temperature gradient of 600 mK, a sizable power of 0.3-0.7 fW was measured at 25 mK bath temperature for different load resistances and with an external magnetic field that maximizes the induced exchange interaction. The maximum power of 0.7 fW was measured on a load resistance of 50 k Ω , which is compatible with the tunnel barrier resistance. The power then decreases at large load resistances down to 0.3 fW that was measured at 500 k Ω . The bath temperature strongly affects the heat engine power with a non-monotonic behaviour characterized by a maximum heat conversion at 400 mK. Notably, thanks to the ferromagnetism of the



EuS, a visible power ($\sim 0.1 - 0.2\text{fW}$) was extracted also without the application of an external magnetic field. This confirms the ability of this technology to operate without the need of external fields. Finally, a rough estimation of the engine efficiency can be obtained from the ratio between P_L and the injected heating power $P_{in} = R_{Co}I_H^2$. With such definition an efficiency of $\sim 3 * 10^{-8}$ has been estimated. Higher efficiencies could be reached by reducing the power losses to the substrate.

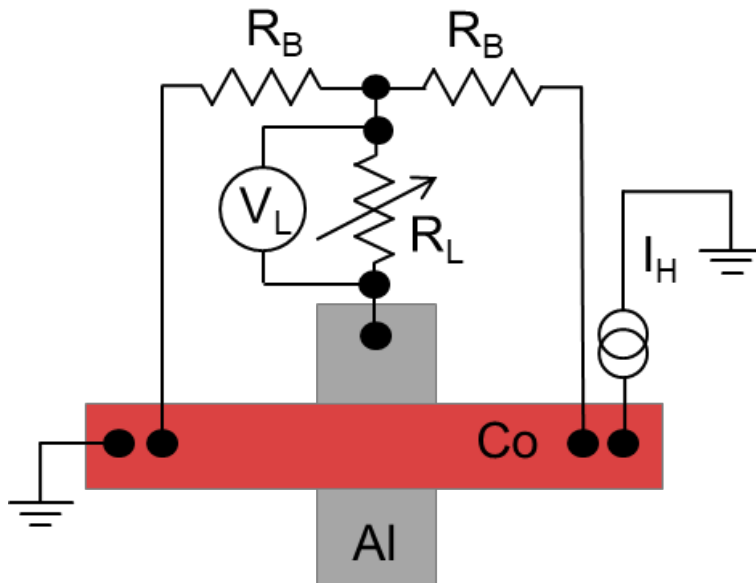


Figure 3: Circuit configuration used for the heat engine measurement with the heating current (I_H) applied on the Co strip, with length (L) and width (W). Equal resistance balances (R_B) were inserted in the circuit to prevent the I_H from passing through the junction when a voltage load (V_L) is measured on the variable load resistance connected to the Al strip.

3 Conclusion

In summary, we have performed characterizations on superconductor-ferromagnetic tunnel junctions made of Al which is proximized by europium sulfide and separated from a Co electrode by an Al oxide tunnel junction. Our devices present reasonably large negative tunnel magnetoresistance, allowing measurements of open circuit thermovoltages when submitted to a temperature difference, which are achieved here by heating currents applied in the Co strip. The different coercivity of the ferromagnets utilized and the large remanence of Co, warrant two important features: the effect is observed even at zero magnetic field and the switching between positive and negative thermovoltages, achieved in the antiparallel configuration on a small range of fields around the coercivity.

The main part of the results presented is the observation of the heat engine effect which was measured for a series of external load resistances. We were able to show the evolution of power released from the junction at different bath temperatures and observe the heat engine efficiency on different load resistances. The overall low efficiency measured is probably due to the heat loss to the substrate which makes the power input much higher than the efficient power on the junction. Several strategies could be performed in order to increase the efficiency in a possible technological application, such as decreasing the junction size or tuning the heat loss by substrate improvements, like bridge utilization for device suspension.



References

1. Meservey, R. & Tedrow, P. M. Spin-polarized electron tunneling. *Physics Reports* **238**, 01124, 173–243. ISSN: 0370-1573. <http://www.sciencedirect.com/science/article/pii/0370157394901058> (2014) (Mar. 1994).
2. Ozaeta, A., Virtanen, P., Bergeret, F. & Heikkilä, T. Predicted very large thermoelectric effect in ferromagnet-superconductor junctions in the presence of a spin-splitting magnetic field. *Physical review letters* **112**, 057001 (2014).
3. Heikkilä, T. *et al.* Thermoelectric radiation detector based on superconductor-ferromagnet systems. *Physical Review Applied* **10**, 034053 (2018).
4. Ullom, J. N. & Bennett, D. A. Review of superconducting transition-edge sensors for x-ray and gamma-ray spectroscopy. en. *Superconductor Science and Technology* **28**. Publisher: IOP Publishing, 084003. ISSN: 0953-2048. <https://doi.org/10.1088/0953-2048/28/8/084003> (2021) (July 2015).
5. Baselmans, J. Kinetic Inductance Detectors. en. *Journal of Low Temperature Physics* **167**, 292–304. ISSN: 1573-7357. <https://doi.org/10.1007/s10909-011-0448-8> (2023) (May 2012).
6. Heikkilä, T. T., Silaev, M., Virtanen, P. & Bergeret, F. S. Thermal, electric and spin transport in superconductor/ferromagnet/insulator structures. *Progress in Surface Science* **94**, 100540 (2019).
7. Strambini, E. *et al.* Superconducting spintronic tunnel diode. en. *Nature Communications* **13**. Number: 1 Publisher: Nature Publishing Group, 2431. ISSN: 2041-1723. <https://www.nature.com/articles/s41467-022-29990-2> (2022) (May 2022).

